Single-Shot Electron Radiography Using a Laser-Plasma Accelerator

G. Bruhaug,[1,2] M. S. Freeman,[3] H. G. Rinderknecht,[1] L. P. Neukirch,[3] C. H. Wilde,[3] F. E. Merrill,[3] J. R. Rygg,[1,2,4] M. S. Wei,[1] G. W. Collins,[1,2,4] and J. L. Shaw[1]

[1]Laboratory for Laser Energetics, University of Rochester
[2]Department of Mechanical Engineering, University of Rochester
[3]Los Alamos National Laboratory
[4]Department of Physics and Astronomy, University of Rochester

To investigate the physical structure of compressed targets, laser-generated x-ray[1,2] or proton radiography[3–5] is typically used, with protons providing the extra feature of electromagnetic field sensitivity. Although x-ray and proton probes are the standard laser-generated diagnostic, there is another laser-generated probe that has seen little use: namely, relativistic electrons. Small-scale high-energy-density (HED) research facilities have performed electron radiography of ultrafast laser–plasma interactions,[6] but this capability has never before been extended to kJ- or MJ-class facilities. The work presented in this summary builds upon previous electron radiography (eRad) work using radio-frequency (rf) linear accelerators[7–9] and small-scale lasers[6–10] and extends it to kJ-class facilities via the already available picosecond lasers for electron-beam generation using a laser-plasma accelerator (LPA).[11,12]

Here, we report the first single-shot eRad images using an electron beam from a 100-J-class LPA. Both contact and projection radiography images of static targets were obtained in materials ranging from plastic to tungsten, and resolutions as good as 90-μm were achieved. This work lays the foundation for future electron radiography of laser-driven targets at kJ- and MJ-class facilities.

Radio-frequency–powered linear accelerators generate monochromatic, low-emittance electron beams suitable for high-quality electron radiography.[7–9] Such systems are rarely available, however, at the same facilities as large HED drivers and cannot easily be installed for experiments due to cost and space constraints. Nevertheless, these HED facilities often have ps lasers available, such as the OMEGA EP, NIF-ARC, PETAL, and Z-Petawatt lasers, which can be used to efficiently generate relativistic electron beams via LPA techniques.[11] This method could allow electron beams to be generated for radiography without needing to add a large and costly rf linear accelerator to an HED facility. A laser-driven eRad system also possesses the temporal characteristics that could make it an ideal diagnostic of other picosecond-scale processes for which linear accelerators do not provide sufficient instantaneous electron flux.

Electron radiography provides a complementary probe to existing x-ray and proton radiography techniques. Unlike laser-generated protons, laser-generated electrons are able to penetrate more material at a given energy. For example, a typical laser-generated 15-MeV proton will be fully stopped by ~2 mm of plastic at standard density and temperature, while a 15-MeV electron will require multiple centimeters of plastic to be fully stopped.[13] Relativistic electrons are also more sensitive to magnetic fields than protons for a given energy, but less sensitive to electric fields. This makes electrons an excellent complement to protons for radiography of electromagnetic fields.

The experiments were performed using the OMEGA EP LPA electron beam[11] and performed in both contact and projection radiography configurations (see Fig. 1).

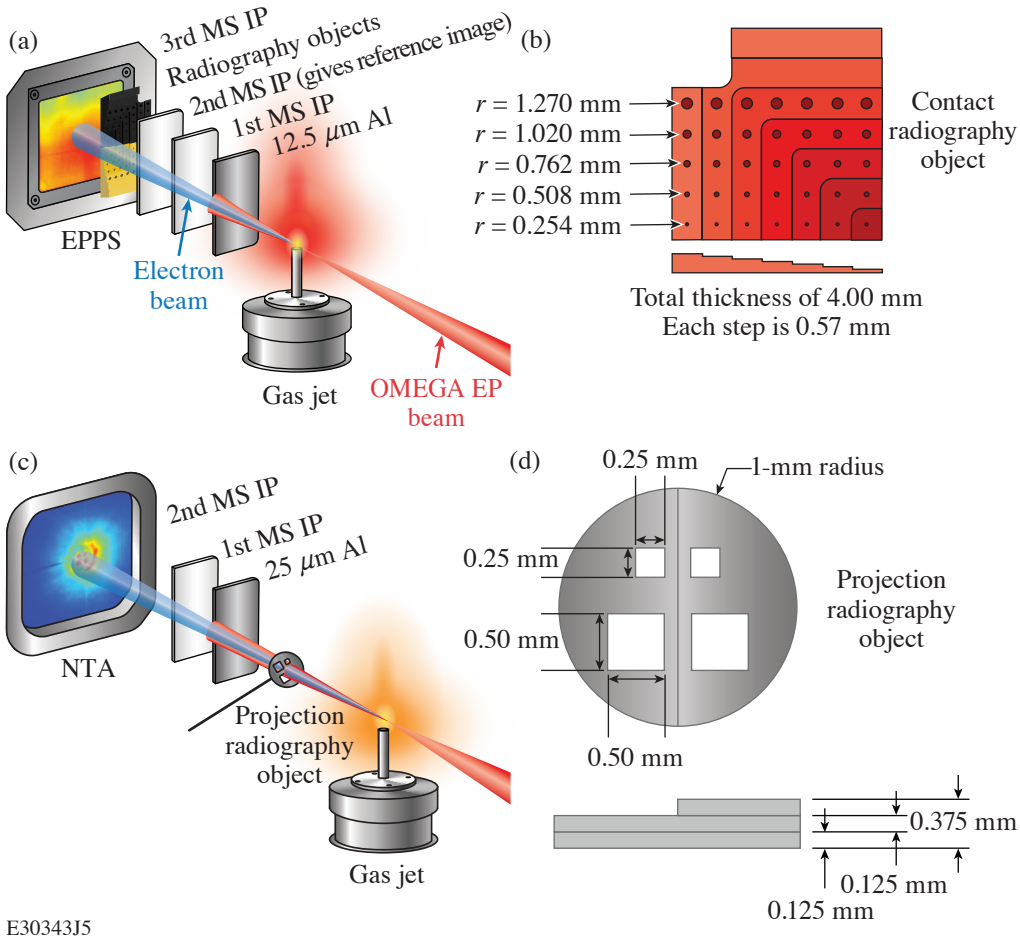

Figure 1
(a) Experimental setup for contact LPA eRad using radiography test objects (b) placed directly onto image plates and (c) projection LPA eRad using 2-mm-diam radiography test objects (d) offset from the image plates by distances ranging from 3.58 to 33.58 cm. MS IP: MS image plate; EPPS: electron–positron–proton spectrometer; NTA: near target arm.

Objects ranging from plastic to tungsten were radiographed at a wide variety of distances and thicknesses. This allowed testing the effect of target Z, density, thickness, and target magnification. The results of contact radiography can be seen in Fig. 2 and projection radiography in Fig. 3.

Resolutions nearing 90 μm were seen, but with little variation in magnification or target material. The resolution degraded with target thickness as expected, but nearly 4 mm of tungsten were able to be radiographed successfully. This shows the extreme penetrative capability of this new diagnostic platform. Laser-induced electric fields in projection radiography were also measured and found to be ~1 GV/m, which is in line with previous literature on the topic.[14]

This material is based upon work supported by the Department of Energy National Nuclear Security Administration under Award Number DE-NA0003856, the University of Rochester, and the New York State Energy Research and Development Authority.

1. E. L. Dewald *et al.*, Rev. Sci. Instrum. **89**, 10G108 (2018).
2. C. Courtois *et al.*, Phys. Plasmas **18**, 023101 (2011).
3. J. R. Rygg *et al.*, Science **319**, 1223 (2008).

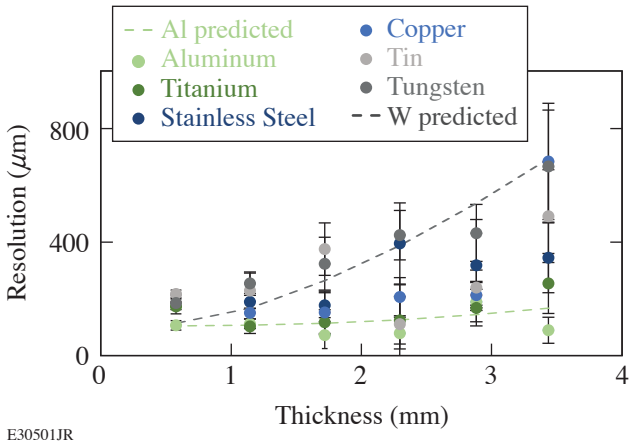

Figure 2
Average measured resolution of contact radiography test object versus target thickness. Theoretical predictions[15] for the tungsten and aluminum are included to guide the eye at the extremes of contact radiography test object *Z* numbers. The error bars are calculated using standard deviation between any repeat radiographs of the same target.

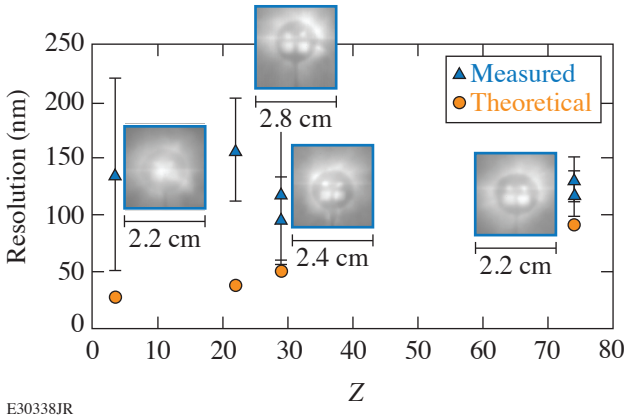

Figure 3
Resolution versus atomic number (*Z*) of the target material for the projection configuration when the image plate was 8 cm from the location of the best laser focus. Each data point has the radiograph recorded on the image plate next to it. Resolution is measured at the edges of each hole in the object as well as the outer edge. Error bars were calculated via the standard deviation between the resolution measurements on the same object.

4. A. B. Zylstra *et al.*, Rev. Sci. Instrum. **83**, 013511 (2012).
5. C. K. Li *et al.*, Phys. Plasmas **16**, 056304 (2009).
6. W. Schumaker *et al.*, Phys. Rev. Lett. **110**, 015003 (2013).
7. F. E. Merrill, Laser Part. Beams **33**, 425 (2015).
8. F. E. Merrill *et al.*, Appl. Phys. Lett. **112**, 144103 (2018).
9. F. Merrill *et al.*, Nucl. Instrum. Methods Phys. Res. B **261**, 382 (2007).
10. D. Hazra *et al.*, Phys. Rev. Accel. Beams **22**, 074701 (2019).
11. J. L. Shaw *et al.*, Sci. Rep. **11**, 7498 (2021).
12. F. Albert *et al.*, Nucl. Fusion **59**, 032003 (2018).
13. M. J. Berger *et al.*, (2017), *ESTAR*, *PSTAR*, and *ASTAR*: Computer Programs for Calculating Stopping-Power and Range Tables for Electrons, Protons, and Helium Ions (Ver. 2.0.1). [Online] Available: https://www.nist.gov/pml/stopping-power-range-tables-electrons-protons-and-helium-ions [17 August 2018].
14. J. L. Dubois *et al.*, Phys. Rev. E **89**, 013102 (2014).
15. A. Nassiri, Argonne National Laboratory, Urbana, IL, Report LA-165 (1991).